Photogrammetry analysis of a vacuum-membrane solar dish using elliptical television antennas

Cite as: AIP Conference Proceedings **2445**, 120021 (2022); https://doi.org/10.1063/5.0087025
Published Online: 12 May 2022

Jonathan K. Swanepoel, Casey Roosendaal and Willem G. le Roux

Photogrammetry Analysis of a Vacuum-Membrane Solar Dish Using Elliptical Television Antennas

Jonathan K. Swanepoel, Casey Roosendaal and Willem G. le Roux [a)]

Department of Mechanical and Aeronautical Engineering, University of Pretoria, Private Bag X20, Hatfield, Pretoria, 0028, South Africa

[a)] Corresponding author: willem.leroux@up.ac.za

Abstract. The design of a solar dish usually involves the complex trade-off between cost and optical quality. The use of off-the-shelf elliptical television antennas in a vacuum-membrane solar dish array is investigated in this paper, in an effort to reduce the cost of solar concentration. Each facet comprised a 50-µm-thick Mylar sheet membrane, stretched and sealed over the elliptical rim of an off-the-shelf satellite television antenna, forming a narrow cavity in which a vacuum could be drawn to pull the Mylar sheet into a concave shape. The shape of the facet concavity was investigated using photogrammetry. An elliptic paraboloid and a hemi-ellipsoid were fitted to the photogrammetry results, and it was determined that both fits could be used to represent the concave shape. The investigation allowed for the concave shape to be modelled in a ray tracing analysis, where the flux map was compared with the result from a lunar flux mapping analysis. Comparison of the intercept factor trends showed that further investigation into quantifying the contributions of individual facet alignment errors should be performed to further improve the model. With improvements in individual facet alignment, the use of off-the-shelf elliptical television antennas in a vacuum-membrane solar dish array can be a viable solution to reduce the cost of solar concentration.

INTRODUCTION

(a) (b) (c)

FIGURE 1. Multi-faceted reflector with facets not aligned (a), target board during lunar testing with aligned (aimed) facets (b) and single facet photogrammetry setup (c).

Solar dish concentration based on elliptical vacuum membrane facets has recently been investigated by Zangeneh et al. [1] and Schmitz et al. [2]. In a solar dish array, facets with elliptical rims can deliver higher optical efficiency than circular facets [1]. A common issue faced with solar dish design is the trade-off between cost and optical quality [3]. A low-cost multi-faceted CSP collector is therefore being developed at the University of Pretoria (see

SolarPACES 2020
AIP Conf. Proc. 2445, 120021-1–120021-9; https://doi.org/10.1063/5.0087025
Published by AIP Publishing. 978-0-7354-4195-8/$30.00

Fig. 1a), where each facet comprises a reflective polymer membrane stretched over the elliptical rim of a television antenna dish [4]. According to Good et al. [5], the specularity error of Mylar can be as low as 0.05 mrad. According to Coventry and Andraka [3], a typical slope error for Mylar stretched-membrane facets is 1.5-2.5 mrad, while it is 2.5-3.5 mrad for stainless steel stretched-membrane facets. Coventry and Andraka [3] further reported that the CSP industry has found it difficult to achieve low-cost manufacturing methods for stretched-membrane facets [3]. Off-the-shelf television dishes are available at low cost because of bulk manufacturing and are therefore investigated in this work for low-cost manufacturing of stretched-membrane facets. Vacuum-membrane reflector facets are known to decrease weight on CSP collectors and provide a degree of optical control because of increased modularity [6]. In order to perform a numerical simulation of the multi-faceted CSP collector which can be compared with the result from a lunar flux mapping analysis (see Fig. 1b), the shape of the concavity formed by the reflector membrane under vacuum should be determined. This paper presents the method that was followed to numerically define the shape of the vacuum-membrane facets and the modelling thereof.

FACET DESIGN

The elliptical rim of the investigated satellite television antenna has a minor axis length of 757.5 mm and a major axis length of 820 mm. A pneumatic valve, comprising a 1/4-inch, threaded nipple, a quarter-turn valve and an 8 mm hose nipple was inserted into the back of the dish, through which a vacuum could be drawn [4,7]. All the connections at the back of the dish, including the dish mount and the pneumatic valve, were sealed with general-purpose silicone to prevent leaks. The 50-µm-thick Mylar sheet was cut from an 8 m × 1.2 m Mylar roll using a 1030 mm × 1100 mm fabricated elliptical template. Sixteen steel couplets were inserted along the Mylar sheet's perimeter at equal angles, through which a tensioning nylon rope would pull the sheet into equal tension using a tensioning frame, as shown in Fig. 2. A generous amount of SikaTack windscreen silicone was run along the rim of the satellite dish, which was pressed onto the tensioned Mylar sheet, allowing the windscreen silicone to form an airtight seal between the Mylar sheet and the satellite dish. The dish's weight was the only force pushing down on the sheet, which resulted in an evenly tensioned reflector facet that had no wrinkling in the non-vacuum state. It was important to ensure that the Mylar sheet was tensioned evenly to negate wrinkling once the satellite dish was applied. Uneven tensioning of the Mylar sheet would mean that the resulting image at the receiver aperture would be distorted and inaccurate.

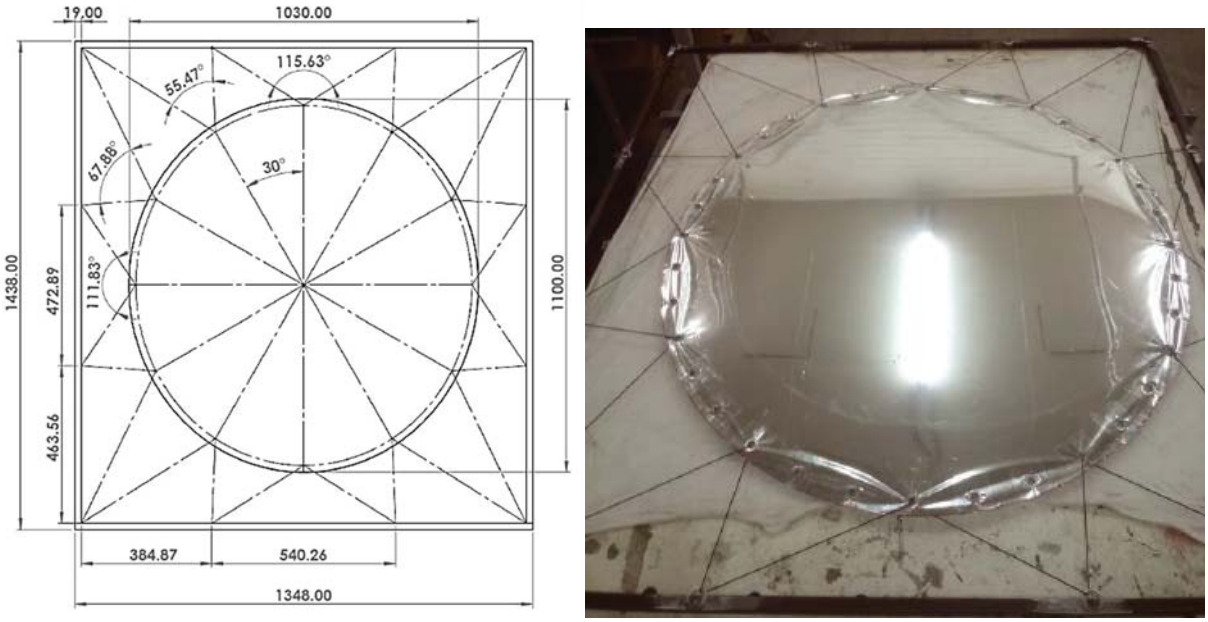

(a) (b)

FIGURE 2. Mylar sheet tensioning frame: (a) schematic; and (b) photograph.

METHODOLOGY

Photogrammetry Analysis

In order to determine the vacuum-drawn membrane shape of the elliptical facets, a digital photogrammetry analysis was performed. Following the work of Dähler et al. [8], the shape of the vacuum-membrane was captured using the GOM ARAMIS Adjustable 4M System. The ARAMIS system is primarily used to measure deformations in a material by determining the relative displacements of certain identified features between two camera shots and transforming them into relative cartesian coordinates. The first camera shot is taken of the initial state of the material and the second is taken of the deformed material [9]. The cameras used in the GOM ARAMIS system can take photos at a quality of 4-megapixels and at a rate of 60 frames per second. The testing was carried out at camera settings of 4-megapixel quality and 1 frame per second.

Multiple place markers were positioned across the surface of the reflector facet, as well as on a position reference point, and photographs were taken of the facet to gauge the relative position of these place markers in non-vacuum (flat) and vacuum (concave) conditions. The place markers were round, white adhesive polymer stickers which were 15 mm in diameter and had a 3 mm black border around the circumference of the sticker to aid in contrast. The markers were positioned in a random pattern on the Mylar sheet (see Fig. 1c) and were placed at position reference points that extended from the side of the facet. The position reference points were solid structures that would not move with the Mylar membrane as a vacuum was formed within the facet cavity. They served as position calibration markers to mitigate errors occurring from the unintentional movement of the photogrammetry cameras.

A self-developed Python code was used to read the cartesian coordinates and transform the shape to the respective origins of the cartesian plane [7]. This was done by obtaining three place markers positioned along the rim of the facet and determining the transformations required to align the normal unit of the displacement vectors of the place markers to be parallel to the z-axis. This was achieved using a three-dimensional (3D) transformation matrix and the Nelder-Mead optimisation algorithm [10]. In order to estimate the true shape of the Mylar sheet under a vacuum condition, two 3D surfaces were investigated by fitting them to the cartesian coordinates (x, y and z) from the photogrammetry analysis. These surfaces were elliptic paraboloid (Eq. 1) and hemi-ellipsoid (Eq. 2) of which the respective surfaces are mathematically defined below. The a-coefficients define the shape of the surface, while the b-coefficients define the location of the surface in the cartesian system.

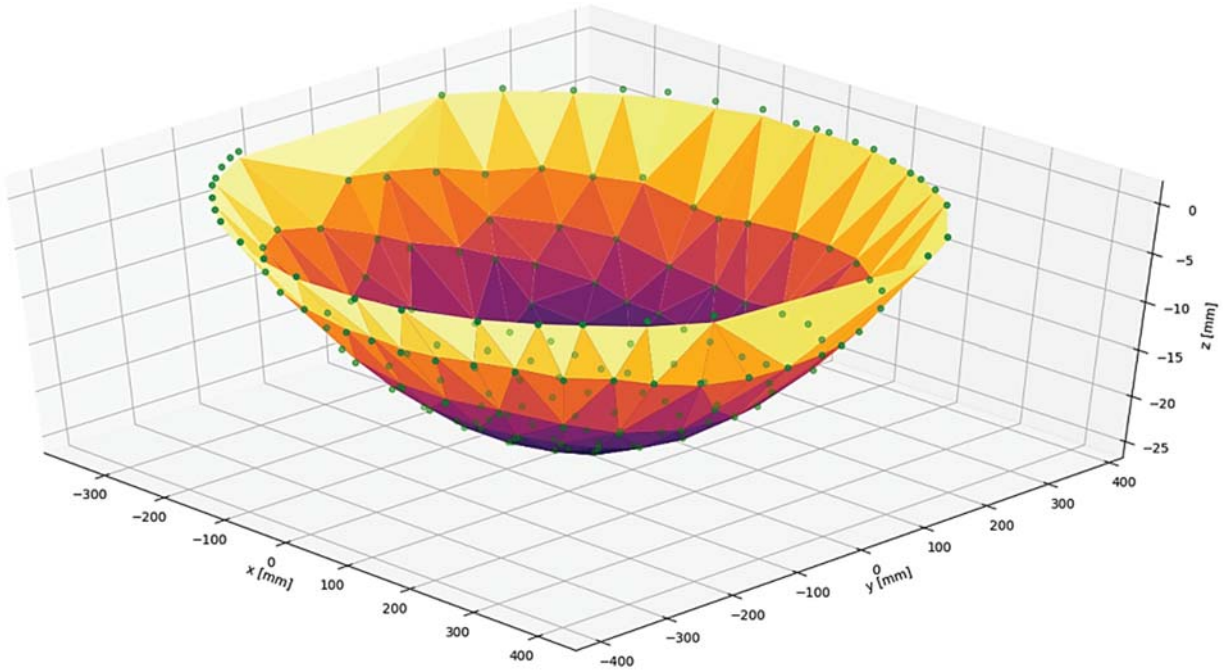

FIGURE 3. Surface fit of the hemi-ellipsoid to the photogrammetry coordinates.

$$z(x,y) = \frac{(x+b_1)^2}{a_1^2} + \frac{(y+b_2)^2}{a_2^2} - b_3 \quad (1)$$

$$z(x,y) = a_3\sqrt{1 - \frac{(x+b_1)^2}{a_1^2} + \frac{(y+b_2)^2}{a_2^2}} - b_3 \quad (2)$$

An illustration of the resulting surface fit of the hemi-ellipsoid to the photogrammetry coordinates is presented in a surface plot in Fig. 3. Since the surface fit of the elliptic paraboloid is effectively indistinguishable from that of the hemi-ellipsoid, the elliptic paraboloid surface plot is not presented here. Scaling in the illustration is magnified in the *z*-direction in order to observe the shape of the surface and photogrammetry coordinates. This means that the errors are also magnified. They are apparent around the rim of the dish. The root mean square (RMS) was applied to the errors between the photogrammetry coordinates and each fitted surface and was minimised by adjusting the equation coefficients using the COBYLA optimization algorithm [11].

Ray Tracing Analysis

Based on the results of the photogrammetry method, the optical surfaces of the facets were modelled in SolidWorks (CAD software) using the satellite television antenna dimensions and facet layout presented by Roosendaal et al. [4]. The alignment (aiming) of the facets also took place in the SolidWorks model. Arbitrary membrane depth and tilt angles were first investigated in SolTrace for a generic circular facet with a spherical surface and then for the elliptical facet shown in Fig 1c, assuming a 4.65 mrad pillbox sun shape and no optical errors (zero slope and specularity errors). A SolidWorks ray tracing model was then validated against the SolTrace results in order to easily obtain the optical characteristics of the facets. Correlations were formulated by measuring the focal lengths, membrane depths, and lateral displacements when tilted for various configurations of the SolidWorks model. The SolidWorks model streamlined the process drastically, providing fast and easily obtainable facet characteristics that were required for the accurate aiming of the facets in the array based on each facet's location from the target. This was done by creating relationships between the traced rays and the membrane surface using basic optical principles. Due to the complex geometry of the vacuumed membrane, the SolidWorks model had to be meshed and imported into SolTrace. The SolidWorks solar reflector model was therefore meshed with triangular elements in ANSYS. Passing the mesh file through a Python script extracted the mesh elements into a series of files which were then imported as surface elements into SolTrace using an import script [12]. The optical surface was thus represented as a series of surface elements with assigned optical properties ready for ray tracing. The flux image in SolTrace was then compared with a lunar image similar to the one shown in Fig. 1b.

RESULTS

Photogrammetry Results

As shown in Fig. 4a and Fig. 4b, the RMS error, used as the objective function, converged after three iterations for the elliptic paraboloid fit and after approximately 150 iterations for the hemi-ellipsoid fit. The RMS error converged to 27.34×10^{-2} mm for the elliptic paraboloid and 24.07×10^{-2} mm for the hemi-ellipsoid. When analysing the resulting error contour plots in Fig. 4c and Fig. 4d, it is evident that both surfaces fit the photogrammetry coordinates in a comparable manner. The error was calculated by determining the difference in the *z*-coordinates between the photogrammetry coordinates and the fitted curves.

The surface fits carry particular errors along the rim of the facet and at coordinate (x, y) = (0, 100). An error of approximately -1 mm is observable along the rim. The error contour plots in Fig. 4c and Fig. 4d show that the *z*-coordinates for the fitted curves diverge from the *z*-coordinates of the actual membrane. The divergence along the rim is believed to have occurred due to the positioning of the markers along the structural rim. Since the rim is a rounded, solid supporting frame, the position references will not change as the vacuum is pulled and will therefore not describe the shape of the concavity appropriately. The error that occurs at coordinate (x, y) = (0, 100), is believed to be due to plastic deformation in the facet from the Mylar sheet coming into contact with the insert of the quarter-turn valve at the base of the satellite dish prior to testing. The plastic deformation causes a concave dimple in the sheet from the vacuum. Thus, the *z*-coordinates of the fitted surfaces are larger than those of the photogrammetry coordinates at this

point. These errors contribute to the accuracy of the surface fits, but, for the majority of the data points, it is apparent that the shape of the concavity that occurs from a thin sheet being pulled over an elliptical rim by a vacuum may be described using either of the surface fits investigated in the research.

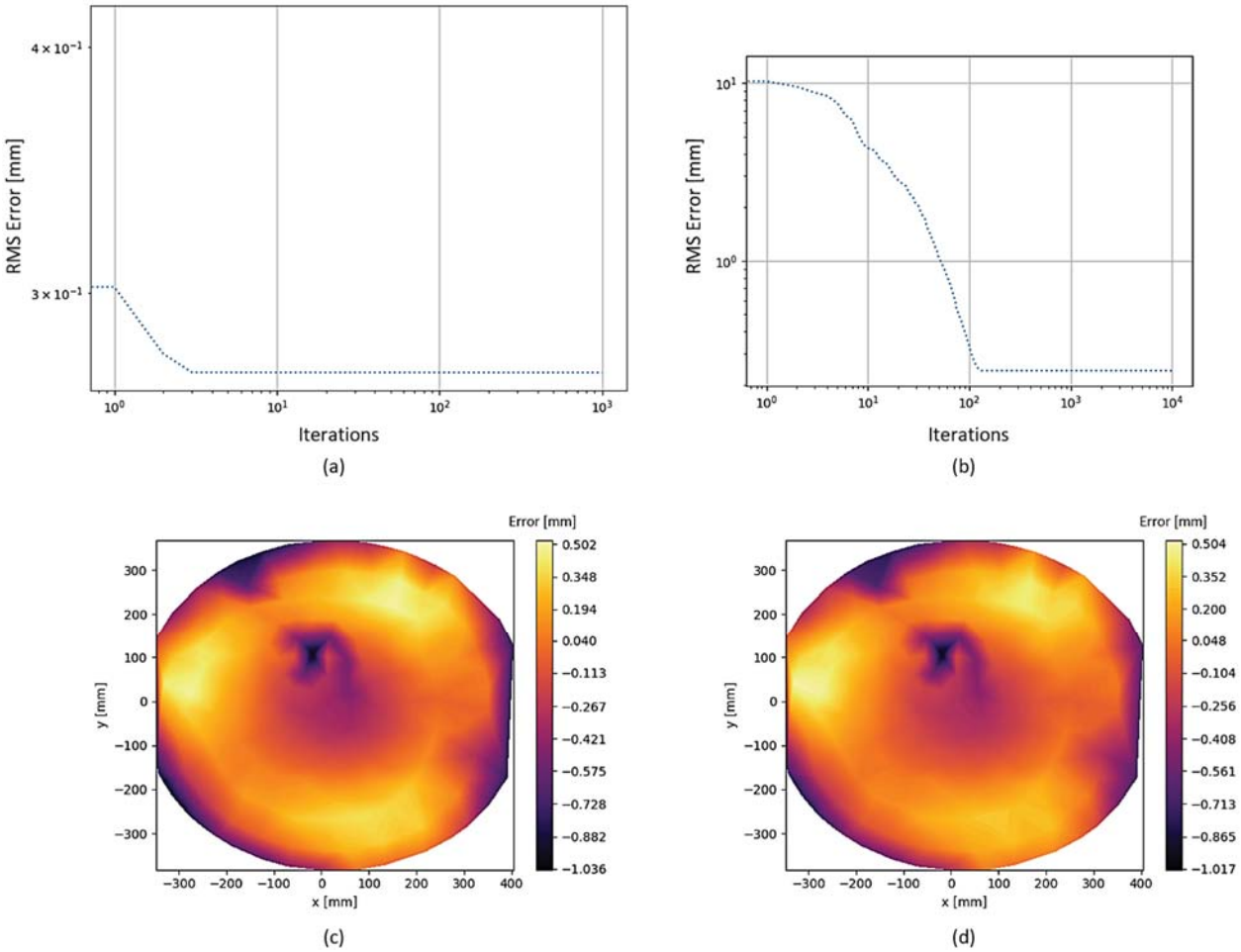

FIGURE 4. Iterations to convergence and resulting error contour plot for the fit of: the elliptic paraboloid, (a) and (c); the hemi-ellipsoid, (b) and (d).

TABLE 1. Resulting coefficients of the fitted surface models.

Coefficients	Elliptic paraboloid	Hemi-ellipsoid
a_1	82.18	1438.07
a_2	76.75	1345.85
a_3	-	-602.65
b_1	26.64	26.74
b_2	-5.6	-5.72
b_3	-24.97	577.73

The resulting equation coefficients for the elliptic paraboloid and the hemi-ellipsoid are presented in Table 1. It should be noted that none of these complex surfaces can be modelled in SolTrace. The hemi-ellipsoid surface described in SolTrace is rotationally symmetric and does not account for the elliptical rim in the current investigation. In order to fully constrain the hemi-ellipsoid surface in the SolidWorks ray tracing model, the surface's shape coefficients would have to be determined as a function of membrane depth. The photogrammetry analysis only presents results for a single membrane depth in Table 1. Further photogrammetry investigation would be required to

determine the shape coefficients of the hemi-ellipsoid surface as a function of membrane depth. In comparison, the elliptic paraboloid surface model was able to be fully constrained by defining the dimensions of the elliptical facet rim (757.5 mm × 820 mm) and the membrane depth. The elliptic paraboloid surface was therefore chosen to be numerically modelled in the SolidWorks ray tracing model.

Ray Tracing Results

Using the results of the photogrammetry analysis, the facets were modelled in SolTrace so that the flux image could be compared with a lunar image similar to the one shown in Fig. 1b. An elliptic paraboloid SolidWorks sketch model shown in Fig. 5, which served as a parametrically-driven ray tracing model, had to be validated first in order to easily obtain the optical characteristics of the facets. The effect of the sun shape is evident in the conical reflected rays in Fig. 5. Correlations were formulated by measuring the focal lengths, membrane depths, and lateral displacements when tilted for various configurations of the SolidWorks model (see Fig. 6).

The meshed dish array reached mesh independence with 5 mm triangular elements and was simulated in SolTrace with 1 000 000 rays and optical errors ranging from 10 mrad to 20 mrad (see Eq. 3 [13]). Some of the steps of this process are shown in Fig. 7a and 7b. The resulting SolTrace normalised flux distribution on a flat surface was then compared with that of the experimental lunar flux map obtained by Roosendaal et al. [4]. The surface data was processed using a Python script to produce contour plots of the normalised flux distribution as well as intercept factor plots.

$$\sigma_{optical} = \sqrt{4\sigma_{slope}^2 + \sigma_{specularity}^2} \tag{3}$$

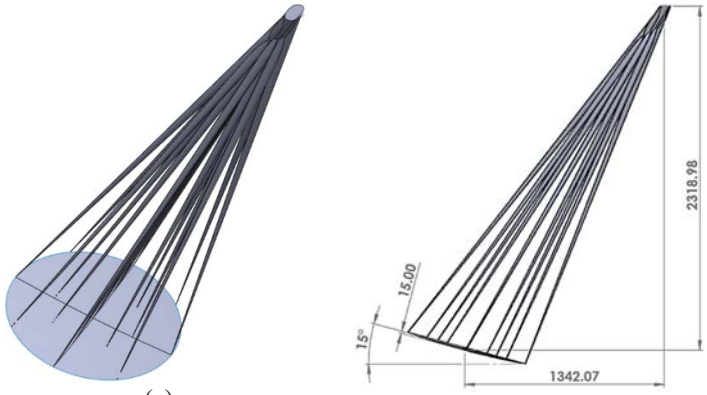

FIGURE 5. SolidWorks ray tracing model of elliptic paraboloid with (a) isometric 3D view and (b) dimensioned view of the facet's major axis.

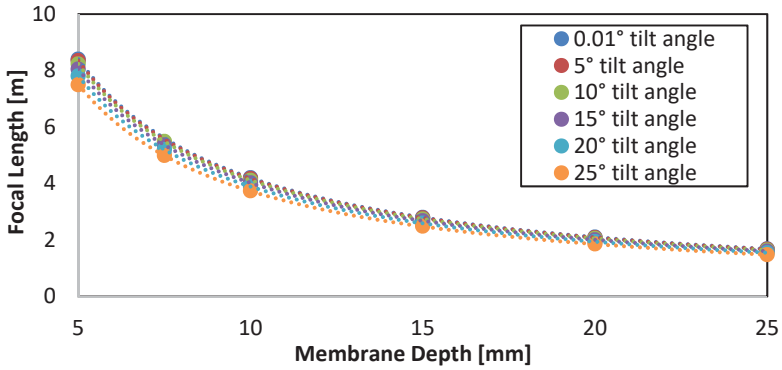

FIGURE 6. Focal length as a function of membrane depth and tilt angle for an elliptic paraboloid membrane surface.

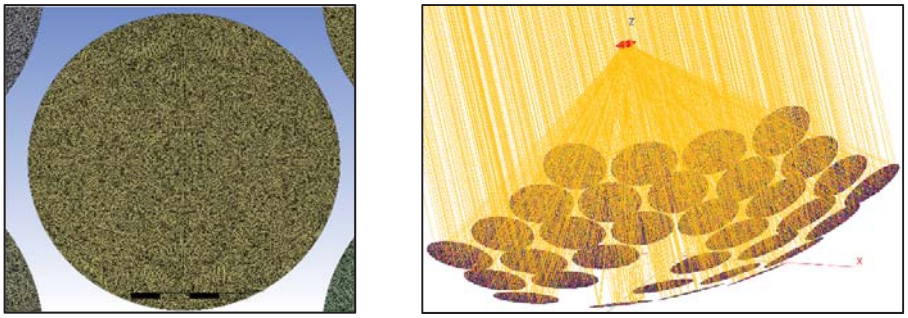

(a) (b)

FIGURE 7. Numerical analysis of elliptic paraboloid facets: (a) Meshed facet in array; and (b) SolTrace ray tracing results.

Running the analytical model with various optical errors produced Fig. 8, where the intercept factors were integrated from the weighted centroid of the flux distribution. With an increase in optical error, the focal image grows and therefore the curve moves towards the left along the *x*-axis. The location of the curve along the *x*-axis and the shape of the curve provide information about the concentrated image. Roosendaal et al. [4] report an intercept factor of 88.6% for a geometric concentration ratio of 249. Fig. 8 shows that a 17.5 mrad optical error produced comparable results to that of the moonlight test by achieving 88.8% intercept factor at the same geometric concentration ratio. However, the curve only matches the location along the *x*-axis but not the profile of the moonlight results. Therefore, another source of error needs to be quantified, namely facet alignment error where the goal is to achieve a single point of focus. This error describes the distribution of high-intensity flux zones on the target surface. Considering the shape discrepancy between the intercept factor plots of the numerical model and that of the moonlight test in Fig. 8, it is evident that the experimental facets possess a lower optical error and a prominent alignment error.

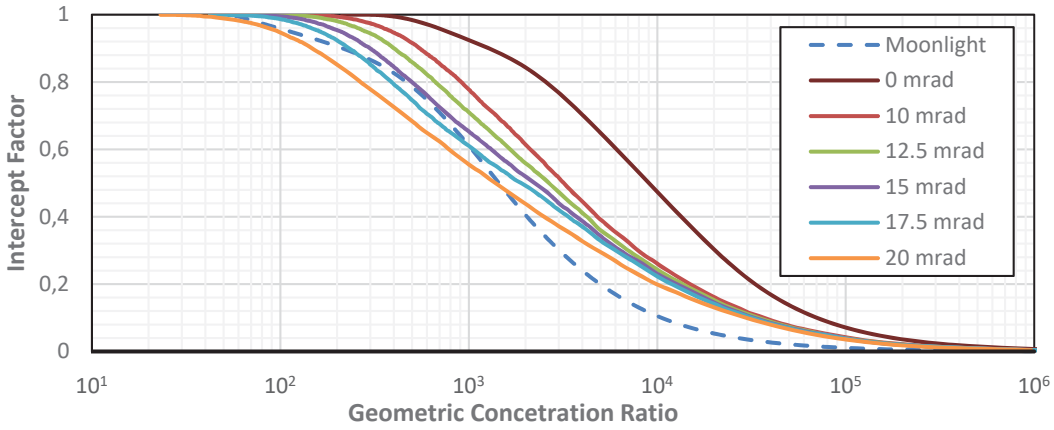

FIGURE 8. Intercept factor versus geometric concentration ratio of the multi-faceted reflector (using meshed elliptic paraboloid facets in SolTrace built in SolidWorks) as a function of optical error. SolTrace flux mapping results are compared with an experimental lunar flux map presented in Ref. [4].

Fig. 9 shows how the light is distributed on the target surface for the moonlight test and the analytical model. Note that the origin of the *x*-axis and *y*-axis is located at the weighted centroid of the flux in Fig. 9a. The centroid in Fig. 9a diverges from the bull's-eye of the target surface in the *y*-axis, which is where the facets were supposed to be focussed. The moonlight flux ratio map (a normalised distribution according to Ref. [4]) has its most intense flux situated around the centroid. It is clear that, for the moonlight test, all the facets were not successfully aimed at the same location on the target surface.

In order to justify the misalignment error, the facets on the parabolic dish were randomly misaligned in the numerical model within a range of +/-0.25 degrees along each lateral axis. The optical error was varied between 0 mrad and 18 mrad. The resulting trends in Fig. 10 conform more accurately to the shape of the moonlight test, highlighting the effect that facet misalignment has on the shape of the intercept factor trend for the moonlight test.

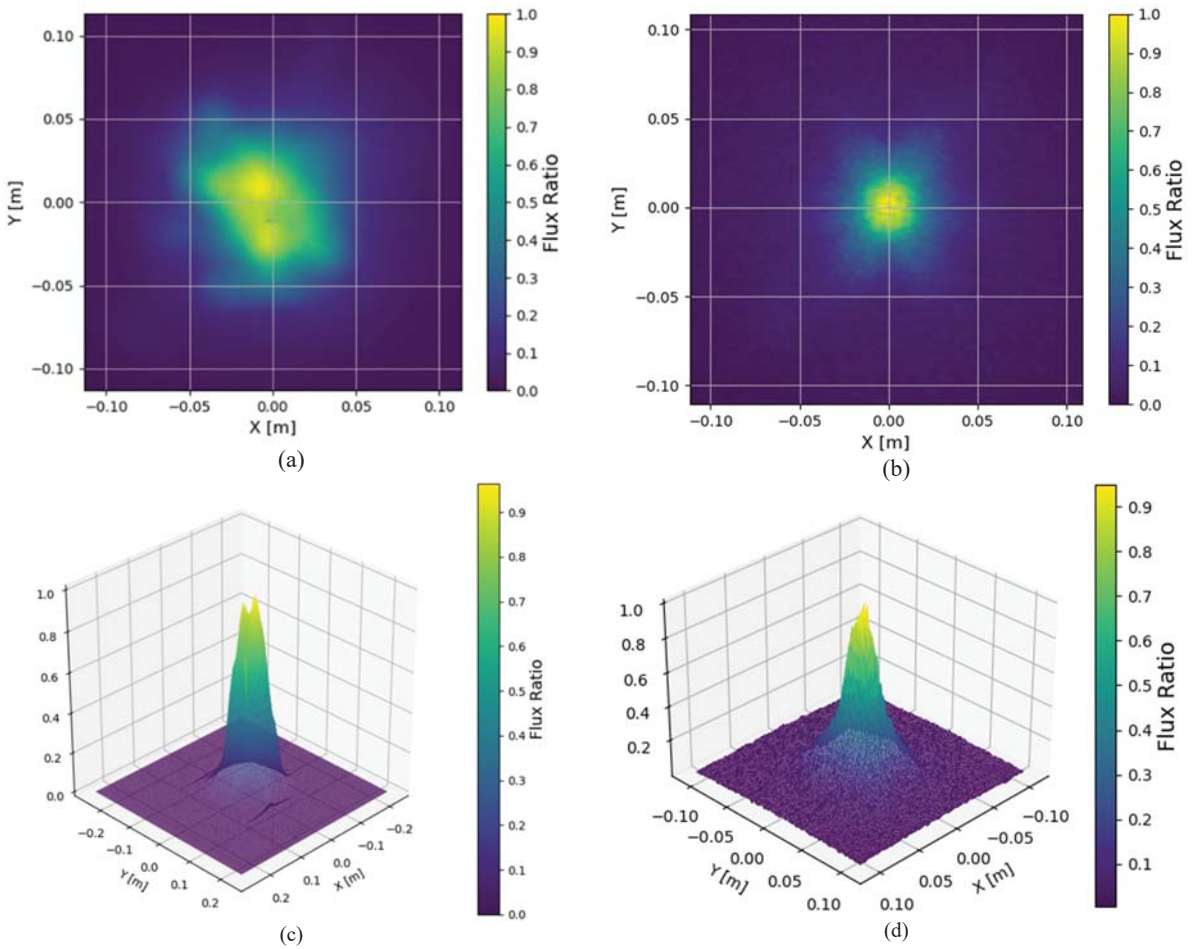

FIGURE 9. Contour plots and 3-D surface plots of the flux ratio for: the moonlight test from Ref. [4], (a) and (c); and the numerical model presented in this work, (b) and (d).

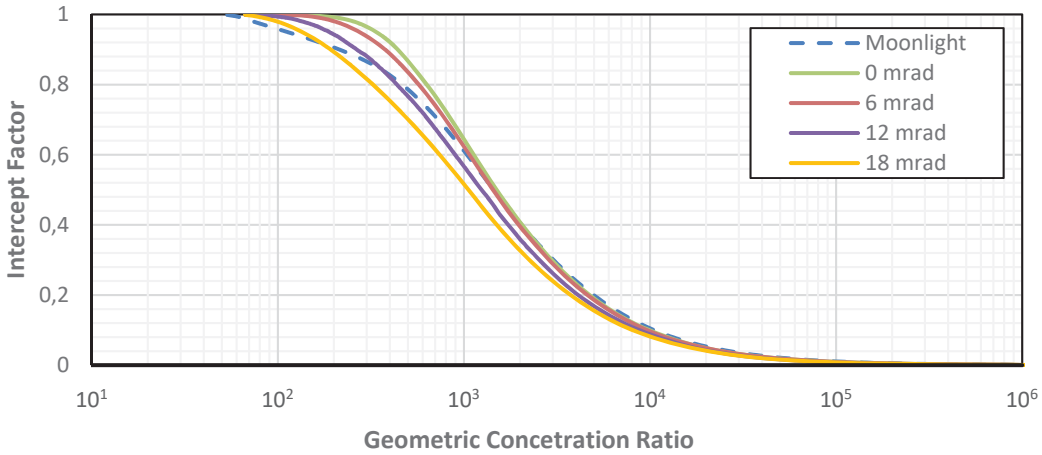

FIGURE 10. Intercept factor versus geometric concentration ratio of the multi-faceted reflector with 0.25-degrees misaligned facets (using meshed elliptic paraboloid facets in SolTrace built in SolidWorks) as a function of optical error. SolTrace flux mapping results are compared with an experimental lunar flux map presented in Ref. [4].

CONCLUSION

The photogrammetry results showed that a hemi-ellipsoid or an elliptic paraboloid represents the shape of the elliptical vacuum-membrane. The results were used to improve the performance of the setup and to identify the effect of optical errors. The analytical investigations into the optical behaviour of a discretised facet with an elliptic paraboloid surface allowed for the successful development of design correlations for a multi-faceted reflector array. Using these correlations, the experimental reflector array in Ref. [4] was numerically modelled and the optical error of the reflector was parametrically investigated. These results were used to identify the sources of error of the experimental reflector shown in Ref. [4]. It was found that an optical error of 17.5 mrad matches the intercept factor result of the moonlight test but is not purely due to slope and specularity error. Comparison of the intercept factor trends showed that an alignment error is apparent in the experimental results. Further investigation into quantifying the contributions of individual facet alignment error and optical error was also performed. The resulting intercept factor plots, with a randomly imposed facet misalignment of up to 0.25 degrees, conformed to the moonlight test result more accurately. With improvements in individual facet alignment, the use of off-the-shelf elliptical television antennas in a vacuum-membrane solar dish array can be a viable solution to reduce the cost of solar concentration.

ACKNOWLEDGMENTS

The authors acknowledge the financial contributions of Innovate UK (Grant Number 105920), the South African Technology Innovation Agency (TIA) and the University of Pretoria's Research and Development Plan (RDP). The financial assistance of the National Research Foundation (NRF) towards this research is also acknowledged (Grant Number 109311). Opinions expressed and conclusions arrived at, are those of the authors and are not necessarily to be attributed to any of the funding bodies mentioned above. The authors also acknowledge the assistance of Mr Leandrew Pestana, Mr George Breytenbach, Mr Marcel Slootweg and Mr Vincent Good.

REFERENCES

1. G. Zanganeh et al., Sol. Energy **86(1)**, 40–47 (2012).
2. M. Schmitz et al., Sol. Energy **153**, 732–743 (2017).
3. J. Coventry and C. Andraka, Sol. Energy **152**, 140–170 (2017).
4. C. Roosendaal et al., Sol. Energy **206**, 200–215 (2020).
5. P. Good et al., Sol. Energy Mater. Sol. Cells **144**, 506–522 (2016).
6. J. R. Bean and R. B. Diver, *Technical status of the dish/stirling joint venture program*. (Sandia National Labs, Albuquerque, NM, 1995); J. Schlaich, Eng. Struct. **21(8)**, 658–668 (1999).
7. J. K. Swanepoel, "Helically coiled cavity receiver for a micro-scale direct generation steam Rankine cycle using a novel solar dish design," MEng Thesis, University of Pretoria, 2019.
8. F. Dähler et al., Sol. Energy **124**, 89–100 (2016).
9. GOM, ARAMIS Adjustable, The modular measuring system for 2D and 3D analyses. Available at: https://www.gom.com/metrology-systems/aramis/aramis-adjustable.html; 2019 [accessed 30.07.2019].
10. J. A. Nelder and R. Mead, Comput. J. **7(4)**, 308–313 (1965).
11. M. J. Powell, *Advances in Optimization and Numerical Analysis* (Springer, Dordrecht, 1994), pp. 51–67.
12. M. Slootweg et al., Sol. Energy **187**, 13–29, (2019).
13. T. Wendelin et al., *SolTrace: a ray-tracing code for complex solar optical systems*. (National Renewable Energy Lab, Golden, CO, 2013).